PCCP

PAPER

View Article Online
View Journal | View Issue

Cite this: *Phys. Chem. Chem. Phys.*, 2018, **20**, 19110

Ab initio design of light absorption through silver atomic cluster decoration of TiO_2†

María Pilar de Lara-Castells, *[a] Carlos Cabrillo,[b] David A. Micha,[c] Alexander O. Mitrushchenkov[d] and Tijo Vazhappilly[e]

Received 4th May 2018,
Accepted 27th June 2018

DOI: 10.1039/c8cp02853b

rsc.li/pccp

A first-principles study of the stability and optical response of subnanometer silver clusters Ag_n ($n \leq 5$) on a TiO_2(110) surface is presented. First, the adequacy of the vdW-corrected DFT-D3 approach is assessed using the domain-based pair natural orbital correlation DLPNO-CCSD(T) calculations along with the Symmetry-Adapted Perturbation Theory [SAPT(DFT)] applied to a cluster model. Next, using the DFT-D3 treatment with a periodic slab model, we analyze the interaction energies of the atomic silver clusters with the TiO_2(110) surface. Finally, the hybrid HSE06 functional and a reduced density matrix treatment are applied to obtain the projected electronic density of states and photo-absorption spectra of the TiO_2(110) surface, with and without adsorbed silver clusters. Our results show the stability of the supported clusters, the enhanced light absorbance intensity of the material upon their deposition, and the appearance of intense secondary broad peaks in the near-infrared and the visible regions of the spectrum, with positions depending on the size and shape of the supported clusters. The secondary peaks arise from the photo-induced transfer of electrons from intra-band valence 5s orbitals of the noble-metal cluster to 3d Ti band states of the supporting material.

1 Introduction

Due to their extraordinary stability and selectivity,[1] bare metal clusters of subnanometer size composed of a few atoms have recently emerged as a new generation of catalysts[2–4] and photocatalysts.[5,6] The synthesis of such molecular-like species has been achieved by kinetic control using an electro-chemical technique without employing surfactants or capping agents.[7] Appealing potential applications of these angstrom size objects have been found in important areas such as the development of cancer therapeutic drugs through intercalation of Ag_3 clusters,[7,8] efficient photocatalytic oxidation,[5] carbon monoxide oxidation by deposited Ag_n and Au_n clusters,[4,9] and hydrogen photo-production by means of Ag clusters adsorbed on gold nanostructures.[6] Realizing these atomic metal clusters as widely used functional materials requires them being stable and accessible through, for example, attachment to solid supports. Moreover, recently developed experimental tools have allowed "soft-landing" conditions in the deposition of metal clusters on solid surfaces to be realized.[10–14] In this work, the stability of deposited Ag_n clusters (with $n \leq 5$) on the TiO_2(110) rutile surface is analyzed.

Titanium dioxide, TiO_2, has wide-ranging and well-known applications in semiconductor photocatalysis (for recent reviews see, *e.g.*, ref. 15 and 16), making it one of the most frequently studied support materials. However, TiO_2 can only be activated by UV irradiation, *i.e.*, by about 5–8% of the solar spectrum. The photocatalytic activity of TiO_2 surfaces is also much influenced by the dynamics of the photo-generated holes and electrons which need to reach the surface to be catalytically active.[17,18] The hole–electron recombination (about 90% of the photo-generated hole–electron pairs) in particular, severely limits the photocatalyst efficiency. As a result, the rate of formation of reaction products divided by the incident photon flow is below 10% in TiO_2-based photocatalysts.[15,19] A successful alternative is to decorate the surface with adsorbed metal nanoparticles.[17,18] They alter the electronic band structure near the surface, increasing the photo-generation of electron–hole pairs very close to the site where the photocatalysis happens. Besides, at the metal–oxide interface a space charge or a depleted region develops that hinders electron–hole recombination. Furthermore, localized surface plasmon resonance (LSPR) at the nanoparticles induces light absorption in the visible region.[17]

[a] *Instituto de Física Fundamental (C.S.I.C.), Serrano 123, E-28006, Madrid, Spain. E-mail: Pilar.deLara.Castells@csic.es*
[b] *Instituto de Estructura de la Materia (C.S.I.C.), Serrano 123, E-28006, Madrid, Spain*
[c] *Quantum Theory Project, Departments of Chemistry and of Physics, University of Florida, 32661-8435, USA*
[d] *Université Paris-Est, Laboratoire Modélisation et Simulation Multi Echelle, MSME UMR 8208 CNRS, 5 bd Descartes, 77454 Marne-la-Vallée, France*
[e] *Theoretical Chemistry Section, Bhabha Atomic Research Centre, Mumbai 400085, India*

† Electronic supplementary information (ESI) available: Complementary results on optimized structures of bare Ag_3 and Ag_5 clusters, Xe- and Ag_2–TiO_2(110) interaction potentials, and the Ag_2–TiO_2(110) interaction. See DOI: 10.1039/c8cp02853b

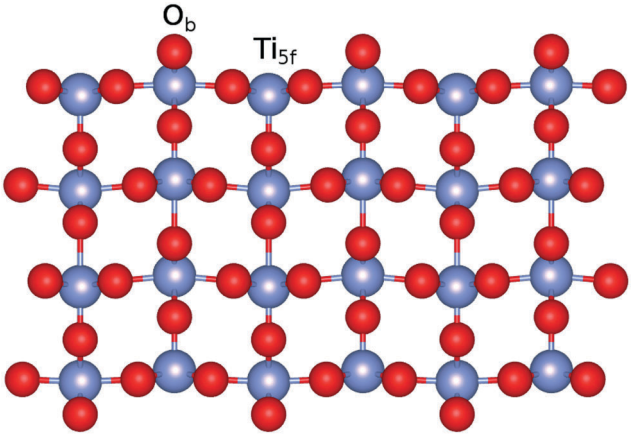

Fig. 1 Figure illustrating a side view of the slab model of the TiO_2(110) surface used in this work. The positions of five-fold (Ti_{5f}) and bridging oxygen (O_b) atoms are also indicated.

Within this context, stable surface attachment of metal atomic clusters opens a very promising new route to photocalytic enhancement of solid surfaces such as those based on TiO_2. Given their atomic scale they are ideally suited for electronic band modification at the very surface, possibly in a profitable way for photocatalytic applications. Indeed, photocatalytic quantum efficiencies increased by three orders of magnitude have already been demonstrated using small Cu clusters.[5] Here, once we have analyzed their stability, we explore, using *ab initio* modelling, such electronic band modification induced by deposited Ag_n clusters (with $n \leq 5$) on TiO_2. Furthermore, with this applicability in mind, we have also calculated the corresponding light absorption spectra in search of prominent solar light absorption, an experimentally verifiable fingerprint to identify promising candidates for the development of photocatalytic and photovoltaic applications.

As far as the stability of the adsorbed atomic clusters is concerned, we have chosen the DFT-D3 method[20,21] among the vdW-corrected DFT treatments after validation using both the domain-based pair natural orbital correlation approach DLPNO-CCSD(T)[22] and the Symmetry-Adapted Perturbation Theory [SAPT(DFT)] method.[23,24] Regarding the electronic band structure calculations, we have relied on the hybrid HSE06 functional[25,26] since it has demonstrated renowned accuracy for TiO_2 band gap calculations. Finally, to calculate the absorption spectra, we use the reduced density matrix (RDM) theory within the Redfield approximation[27] combined with HSE06 calculations. This RDM treatment has been successfully applied to Ag_n clusters adsorbed on semiconductor silicon surfaces.[28–30] In the next section, we briefly present the methods used in this study. Our results are reported in Section 3. Finally, the main conclusions are provided in Section 4.

2 Method

2.1 Structural models

The calculations on the periodic slabs were carried out using the 4 × 2 supercell (four TiO_2 trilayers giving a *ca.* 13 Å width slab) model shown in Fig. 1 and reported in ref. 31. The adsorption of the silver clusters has been modeled on one side of the slab and the vacuum region above the slab was 38 Å thick. This large vacuum region allowed the description of long-range tails of the cluster–surface interaction potentials while avoiding unphysical overlaps of electronic densities. Periodic calculations were carried out by freezing the positions of the O and Ti atoms to those determined by Busayaporn *et al.*[32] using X-Ray Diffraction (XRD). Following ref. 33, the hydrogen-saturated cluster of stoichiometry $Ti_9O_{25}H_{14}$ (see Fig. 2) was used in our finite cluster calculations. The geometry of the model cluster has also been frozen to the experimental geometry of the TiO_2(110)-(1 × 1) surface.[32] Both periodic and cluster structural models have been previously used to study the adsorption of noble gases on the same surface,[34] showing a good agreement for calculated adsorption energies with experimental measurements.[35]

In periodic and cluster calculations, the Ag_2 internuclear distance was fixed to the experimentally determined value[36] (2.531 Å). Complementary results on the optimization of supported and unsupported Ag_2 structures are presented in the ESI.†

2.2 Theoretical approaches using surface cluster models

Using the cluster shown in Fig. 2 to model the Ag_2/TiO_2(110) interaction, the DLPNO-CCSD(T) approach[22] and the SAPT(DFT) method have been applied to assess the performance of the chosen vdW-corrected DFT treatment. The interaction energies were calculated as a function of the cluster–surface distance and included the counterpoise correction[37] to account for the basis set superposition error. The frozen-core treatment was used for 140 chemical core electrons. The SAPT(DFT) method was applied adopting the Perdew–Burke–Ernzerhof (PBE) density functional.[38] This method[23,24,39,40] has allowed the interaction energy to be decomposed as a sum of first- and second-order interaction terms, namely first-order electrostatic E_{elec} and exchange E_{exch}, and second-order induction E_{ind} and dispersion E_{disp} terms, along with their respective exchange corrections ($E_{exch-ind}$ and $E_{exch-disp}$). The δ(HF) estimate[41,42] of the higher-order induction plus exchange–induction contributions was added to the SAPT(DFT) interaction energies. Specifically, the δ(HF) correction is defined as,[41]

$$\delta(\mathrm{HF}) = E_{int}(\mathrm{HF}) - E_{elec}(\mathrm{HF}) - E_{exch}(\mathrm{HF}) - E_{ind}(\mathrm{HF}) \quad (1)$$

where E_{int} is the supermolecular HF interaction energy and the other terms are calculated using the HF density matrices. The dispersion and exchange–dispersion SAPT(DFT) contributions were summed to provide the total exchange–repulsion part, as were the induction, exchange–induction and δ(HF) contributions into the total induction term.

2.3 Theoretical approaches using periodic models

The periodic vdW-corrected PBE-D3 treatment has been applied to calculate interaction energies and optimized geometries after assessing its performance with the DLPNO-CCSD(T) and SAPT(DFT) approaches. Due to the underestimation of the

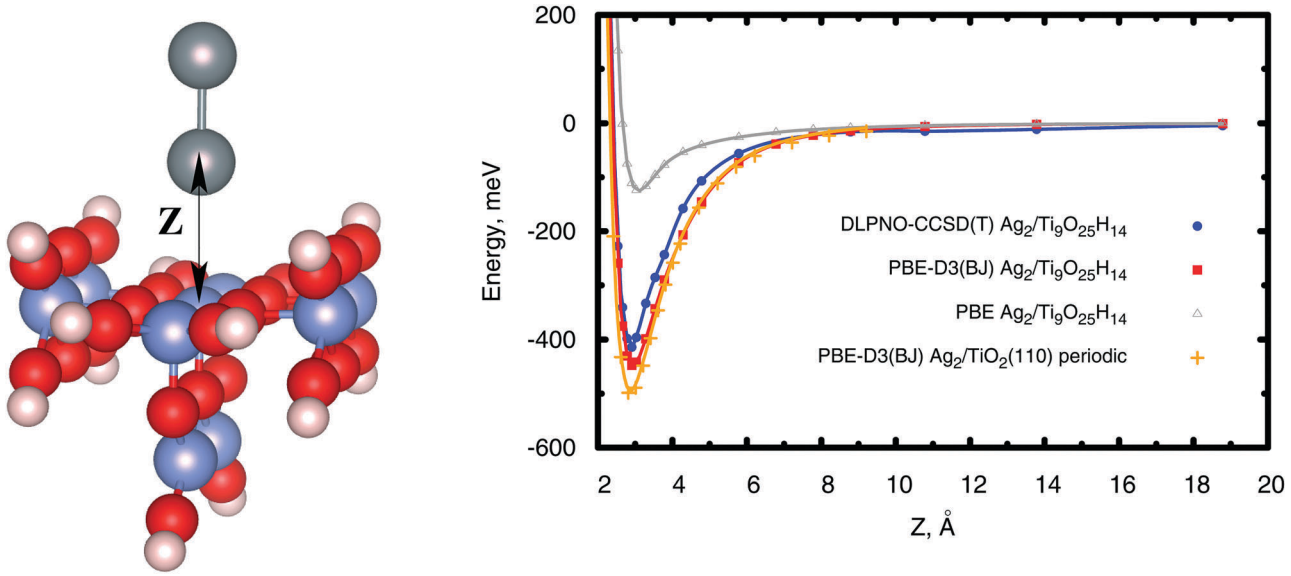

Fig. 2 Left-hand panel: Figure illustrating the hydrogen-saturated $Ti_9O_{25}H_{14}$ cluster modelling the $Ag_2/TiO_2(110)$ system. Gray spheres represent silver atoms while red and blue spheres stand for oxygen and titanium atoms. Hydrogen atoms saturating dangling bonds are also shown with small white spheres. Right-hand panel: Scan of the interaction energies between the Ag_2 dimer and the $TiO_2(110)$ surface using different methods and both cluster ($Ti_9O_{25}H_{14}$) and periodic models of the surface.

band gap from the spurious electron self-interaction in the semilocal PBE treatment, the projected density of states and photo-adsorption spectra were instead calculated with the hybrid HSE06 screened density functional.[25,26] This functional has been chosen because of its capability to provide accurate band gaps of dielectric and semiconductor compounds.[43] It has also been the preferred approach in previous studies of optical and other electronic properties of TiO_2.[44–46] In this work, the HSE06 treatment has provided a direct band gap of 3.26 eV for the $TiO_2(110)$ surface, agreeing very well with experimental measurements for bulk rutile (3.3 ± 0.5 eV).[47]

2.4 Reduced density matrix treatment

2.4.1 Steady state density matrix. In order to calculate light absorption in the system, we model the involved relaxation processes by means of the reduced density matrix (RDM) approach in the Redfield approximation[27] and using an electronic basis set of orbitals generated from DFT calculations.[48,49] When a monochromatic electromagnetic field of frequency Ω is applied, the evolution equation for the RDM, ρ, in the Schrödinger picture reads,

$$\dot{\rho}_{jk} = -\frac{i}{\hbar}\sum_{l}\left(F_{jl}\rho_{lk} - \rho_{jl}F_{lk}\right) + \sum_{l,m} R_{jklm}\rho_{lm} \qquad (2)$$

$$\hat{F} = \hat{F}^{\mathrm{KS}} - \hat{\mathbf{D}}\cdot\mathscr{E}(\mathrm{t}) \qquad (3)$$

$$\mathscr{E}(t) = \mathscr{E}_0(\mathrm{e}^{i\Omega t} + \mathrm{e}^{-i\Omega t}) \qquad (4)$$

where $\hat{F}^{\mathrm{KS}}$ is the effective Kohn–Sham Hamiltonian, the index refers to the Kohn–Sham basis set, $\hat{\mathbf{D}}$ is the electric dipole moment operator and R_{jklm} stand for Kohn–Sham components of the relaxation tensor (Redfield coefficients). The Redfield coefficients are defined as in ref. 27 and are implemented as described in ref. 48. This approximation is valid for medium phenomena relaxing over times that are long compared with transient energy exchange between the adsorbate and its medium.

Within the Redfield approximation used here, the relaxation tensor not only describes the effect of the fast electronic dissipation due to electronic fluctuations in the medium at long times but also the relatively slow relaxation owing to the atomic lattice vibrations. It is convenient to change to a rotating frame accounting for the electromagnetic field oscillation,

$$\tilde{\rho}_{ij}(t) = \rho_{ij}(t)\exp(i\Omega t), \quad \varepsilon_i > \varepsilon_j \qquad (5)$$

$$\tilde{\rho}_{ij}(t) = \rho_{ij}(t)\exp(-i\Omega t), \quad \varepsilon_i < \varepsilon_j \qquad (6)$$

$$\tilde{\rho}_{ii}(t) = \rho_{ii}(t) \qquad (7)$$

where ε_i is the energy of the ith Kohn–Sham orbital. After averaging out over time the fast terms in the equation of motion for the RDM, its stationary-state solution for the diagonal elements reads,[48,50]

$$\tilde{\rho}^{\mathrm{SS}}_{jj} = 2\Gamma_j^{-1}\sum_{k=0}^{\mathrm{HOMO}} g_{jk}(\Omega), \quad j \geq \mathrm{LUMO} \qquad (8)$$

$$\tilde{\rho}^{\mathrm{SS}}_{jj} = 2 - 2\Gamma_j^{-1}\sum_{k=\mathrm{LUMO}}^{\infty} g_{jk}(\Omega), \quad j \leq \mathrm{HOMO} \qquad (9)$$

where LUMO stands for the lowest unoccupied molecular orbital and HOMO denotes the highest occupied one. Γ_j is a depopulation rate and

$$g_{jk}(\Omega) = \frac{\gamma\Omega_{jk}}{\gamma^2 + \Delta_{jk}(\Omega)^2} \qquad (10)$$

Here γ is a decoherence rate, Ω_{jk} are the Rabi frequencies given by $\Omega_{jk} = -\mathbf{D}_{jk}\cdot\mathscr{E}_0/\hbar$ and $\Delta_{jk}(\Omega) = \Omega - (\varepsilon_j - \varepsilon_k)$ are the detunings. The diagonal elements provide the populations of the KS orbitals. The population relaxation rate $\hbar\Gamma$ and the decoherence rate $\hbar\gamma$ were not computed but fixed to values of 0.15 meV and 150 meV (27 ps and 27 fs) and have been chosen to be of the order of rates for semiconductors following decay of phonon and electronic density excitations (see, *e.g.*, ref. 51 for values from measurements of adsorbates on TiO_2).

As far as the populations are concerned, an averaging over many light periods, as happens to be the case in the usual measurements, is equivalent to take the stationary solutions in the rotating frame.[48]

2.4.2 Absorption spectrum. In terms of the stationary populations the absorbance is given by,[29,30,52]

$$\bar{\alpha}(\Omega) = \sum_{j=0}^{\mathrm{HOMO}} \sum_{k=\mathrm{LUMO}}^{\infty} \bar{f}_{jk}\left(\tilde{\rho}_{jj}^{\mathrm{SS}} - \tilde{\rho}_{kk}^{\mathrm{SS}}\right)\frac{1}{\pi}\frac{\hbar\gamma/2}{\left(\hbar\Delta_{jk}\right)^2 + (\hbar\gamma/2)^2} \quad (11)$$

where $\bar{f}_{jk}$ is an oscillator strength per active electron. This is the purely dissipative contribution to the absorbance. We are assuming a thin slab neglecting dispersive effects, *i.e.*, assuming refraction index *ca.* 1. The solar flux absorption spectrum is then given by,

$$F(\hbar\Omega) = \bar{\alpha}(\Omega)F_{\mathrm{solar}}(\hbar\Omega)\hbar\Omega \quad (12)$$

where the solar flux is approximated by the black body flux distribution, normalized to an incident photon flux of 1 kW m^{-2},

$$F_{\mathrm{solar}}(\hbar\Omega) = \frac{(\hbar\Omega)^3}{\pi^3\hbar^3c^3}\frac{C_{\mathrm{T}}}{\exp(\hbar\Omega/k_{\mathrm{B}}T) - 1} \quad (13)$$

with C_{T} the flux normalization constant and the temperature T set to 5800 K.

2.5 Computational details

2.5.1 Surface cluster calculations. Surface cluster calculations were carried out employing correlation-consistent basis sets such as the (augmented) polarized correlation-consistent triple-ζ (aug-cc-pVTZ) basis of Woon and Dunning, Jr.,[53] as reported in ref. 33 for oxygen and titanium atoms, while the aug-cc-pVTZ-PP basis was used for silver,[54,55] including a small-core (19-valence-electron) relativistic pseudopotential.[56] When applying the DLPNO-CCSD(T) and PBE-D3 treatments, the ORCA package of programs[57] was employed (version 4.0.1.2).

The SAPT(PBE) calculations were performed with the MOLPRO package[58] using the density-fitting technique[39] and adopting the same computational setup as ref. 33. The exchange–correlation PBE potential was asymptotically corrected[59] with the ionization potential value reported in the NIST Chemistry Web Book for the silver dimer (7.66 eV from ref. 60). For the cluster model of the TiO_2(110) surface, an ionization potential value of 5.0 eV was chosen on the basis of work function values characterizing TiO_2(110) surfaces[61] (in between 4.9 and 5.5 eV).

2.5.2 Periodic calculations. To perform the periodic calculations, the computational setup reported in a previous study of the He/TiO_2(110) interaction[31] was applied. For this purpose, we used the Vienna *Ab initio* Simulation Package (VASP 5.4.4).[62,63] To describe the electron–ion interaction, the projector augmented-wave method was applied,[63,64] using the PAW-PBE pseudopotentials supplied with the same code. The electrons from O(2s, 2p), Ti(3s, 4s, 3p, 3d) and Ag(4d, 5s) orbitals were treated explicitly as valence electrons. As in ref. 31, we used plane wave basis sets with a kinetic energy cutoff of 700 eV and a Gaussian smearing of 0.05 eV to account for partial occupancies, with the Brillouin zone sampled at the Γ point only. Test calculations showed that interaction energies at the potential minimum using a 5 × 5 × 1 Monkhorst–Pack[65] k-point mesh are within *ca.* 0.005 eV of those calculated at the Γ point (see ESI†).

All interaction energies were determined using the supermolecular approach as follows,

$$E_{\mathrm{int}}^{\mathrm{tot}} = E_{\mathrm{Ag}_n/\mathrm{TiO}_2(110)} - E_{\mathrm{Ag}_n} - E_{\mathrm{TiO}_2(110)} \quad (14)$$

where $E_{\mathrm{Ag}_n/\mathrm{TiO}_2(110)}$ is the total energy of the system, $E_{\mathrm{TiO}_2(110)}$ stands for the energy of the substrate, and E_{Ag_n} denotes the energy of the bare silver cluster.

3 Results and discussion

3.1 Assessment of the PBE-D3(BJ) approach at DLPNO-CCSD(T) and SAPT(DFT) levels

Cost-efficient calculations accounting for the extended nature of cluster–surface systems use vdW-corrected DFT methods. When applying a vdW-corrected DFT approach, benchmarking against accurate reference values is crucial. The coupled-cluster single, doubles and non-iterative triples [CCSD(T)] approach is ideally suited for this purpose. When applied to clusters modelling the TiO_2(110) surface, the incremental method[66] has allowed the CCSD(T) approach to be applied to adsorbate-TiO_2(110) systems (see *e.g.*, ref. 12 and 33), with the employment of localized orbitals making it very efficient. Using the domain-based local pair natural orbital approximation, DLPNO-CCSD(T)[22] is another *ab initio* option that, when applied to molecules adsorbed on TiO_2(110), has provided excellent (within 1 kcal mol^{-1}) agreement with experimental data.[67] In addition, previous work on the He–TiO_2(110) system using cluster models has shown that the SAPT(DFT) approach provides interaction energies very close to those obtained at the CCSD(T) level.[12,33] The incremental approach has been also applied to describe the Ag_2/graphene interaction at the CCSD(T) level,[68] with results showing overall good performance with the PBE-D3 scheme including the Becke-Johnson (BJ) damping of the D3 dispersion correction.[20,21] The PBE-D3 approach has thus been chosen for our periodic calculations while the DLPNO-CCSD(T) and SAPT(DFT) methods are used to validate its adequacy.

From Fig. 2 and Table 1 it can be observed that the PBE-D3(BJ) approach closely reproduces the DLPNO-CCSD(T) and SAPT(DFT) results, with the well-depth values agreeing to within 10%. As can be also seen in Fig. 2, the PBE-D3(BJ) potential energy curves obtained using periodic and cluster models are rather close to each other, confirming the adequacy of both the cluster model and the electronic basis set to provide reference DLPNO-CCSD(T) values.

Table 1 Decomposition of the $Ag_2/(Ti_9O_{25}H_{14})$ interaction energy using the SAPT(PBE) method. Z_e stands for the equilibrium distance between the Ag atom closest to the surface and the five-fold coordinated Ti_{5f} atom (see the left-hand panel of Fig. 2). Well-depths and Z_e values of DLPNO-CCSD(T) and PBE-D3(BJ) potential energy curves are also shown (see the right-hand panel of Fig. 2)

	SAPT(PBE)	DLPNO-CCSD(T)	PBE-D3(BJ)
Z_e, Å	2.86	2.90	2.92
E_{tot}, meV	−429	−414	−447
E_{elec}, meV	−358	—	—
$E_{exch-rep}$, meV	1141	—	—
E_{ind}, meV	−574	—	–
E_{disp}, meV	−648	—	—

Table 1 also shows a SAPT-based decomposition of the total energy to the electrostatic E_{elec}, exchange–repulsion $E_{exch-rep}$, induction E_{ind}, and dispersion E_{disp} contributions. For the perpendicular orientation of the silver dimer, the attractive interaction is dominated by both dispersion and induction contributions, as can be expected from the pronounced polarization of the silver electronic density towards the titania surface. The importance of including dispersion corrections is also clear when comparing PBE and PBE-D3(BJ) interaction potentials, with the well-depth of the former being much smaller (−447 *vs.* −124 meV). The crucial role of the dispersion contribution has been also found for the interaction of silver atomic clusters with a TiO_2 (anatase) surface.[69]

3.2 Interaction potentials and optimized geometries of Ag_n clusters on the TiO_2(110) surface

Once the PBE-D3(BJ) approach has been validated, we analyze the Ag_n–TiO_2(110) interaction by focusing on the supported, not yet explored, Ag_3 and Ag_5 clusters. First, the geometries of the free-standing clusters were optimized at the second-order Möller–Plesset perturbation theory (MP2) level, resulting in isosceles planar triangular (Ag_3) and trapezoidal (Ag_5) structures (see ESI†). These configurations were found as the most stable in previous studies using coupled-cluster approaches.[70,71] A planar trapezoidal structure for Ag_5 was also revealed from experimental observations.[72] Keeping these geometries fixed, Fig. 3 shows scans of the interaction potentials as a function of the adsorbate–surface distance. We have considered two representative adsorption sites in which the cluster center-of-mass is located on top of either the fivefold coordination Ti atom (Ti_{5f} site from now on) or the bridging O atom (O_b site). The energies at the potential minima are presented in Table 2. As can be seen in Fig. 3 (right-hand panel), we have chosen configurations in which the planar structures are oriented perpendicular to the surface plane while the internuclear Ag–Ag (in Ag_2/Ag_3) and Ag–Ag–Ag (in Ag_5) axes lie parallel to the row of Ti_{5f} atoms and O_b atoms. These configurations are found to be more stable for Ag_3 and one Ag_5 isomers (see below). We have also explored configurations for supported Ag_3 clusters which are parallel to the surface plane, providing smaller adsorption energies (by 0.6 eV) when considering the adsorption O_b site. However, the internuclear Ag–Ag axis for the most stable Ag_2

Table 2 Energies (in meV) at the potential minima for the Ag_n–TiO_2(110) interaction, considering Ti_{5f} and O_b adsorption sites (see Fig. 3). Values in parenthesis stand for the vertical distance (in Å) from the Ag atom closest to the plane where the Ti_{5f} atoms are located

Site	Ag	Ag_2	Ag_3	Ag_5
Ti_{5f}	−733 (2.83)	−894 (2.94)	−1811 (2.59)	−1694 (2.61)
O_b	−939 (3.64)	−756 (3.68)	−2251 (3.45)	−2016 (3.42)

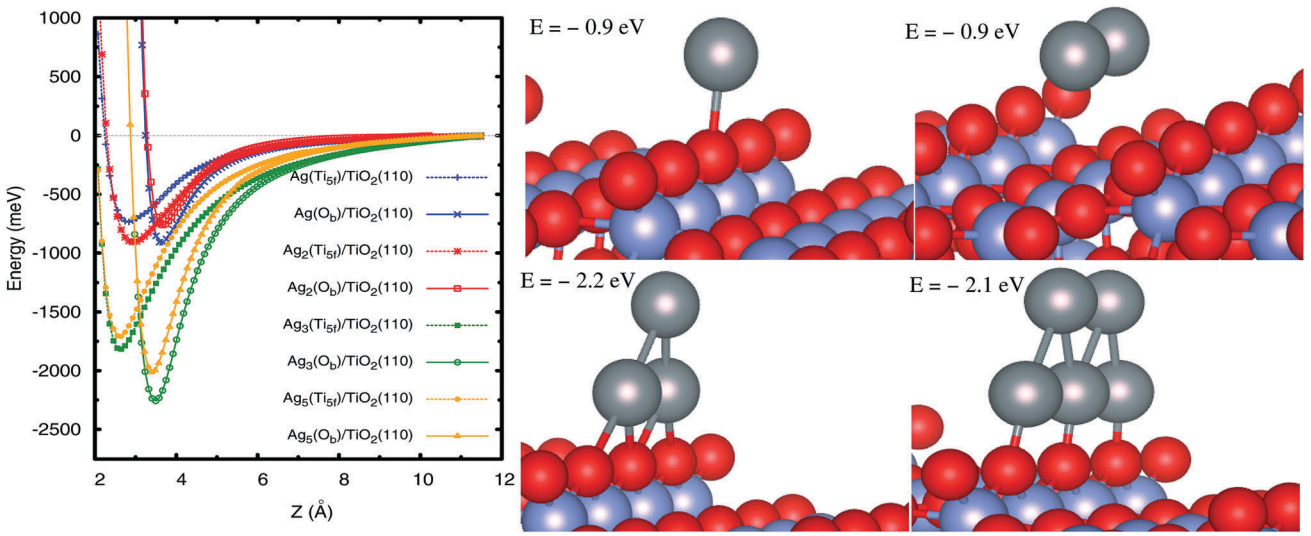

Fig. 3 Left-hand panel: Radial scan of the interaction energies between atomic silver clusters Ag_n and the TiO_2(110) surface, as calculated with the PBE-D3(BJ) method. The cluster center-of-mass is located on top of either the five-fold titanium atom Ti_{5f} (Ti_{5f} site, dashed lines) or the bridging oxygen atom O_b (O_b site, full lines). *Z* stands for the distance between the silver atom closest to the surface and the Ti_{5f} atom along the surface normal direction. Right-hand panel: Geometries of Ag_n clusters on the O_b site. For both adsorption sites, the internuclear Ag–Ag (in Ag_2/Ag_3) and Ag–Ag–Ag (in Ag_5) axes lie parallel to the direction of the row of Ti_{5f} and O_b atoms. Gray spheres represent silver atoms while red and blue spheres stand for oxygen and titanium atoms.

isomer is oriented perpendicular to the Ti_{5f} row, and not shown here. For brevity, complementary results on this structure have been moved to ESI.†

From Fig. 3 it can be observed that the O_b site is clearly favored over the Ti_{5f} position for all Ag_n clusters composed of an odd number of atoms n, with energies at the potential minima differing by up to *ca.* 0.4 eV (see Table 2). The same preferred adsorption site is found at the PBE level, with the D3(BJ) dispersion correction making the energy differences smaller. For instance, for the Ag_3 cluster, the energies of the O_b and Ti_{5f} isomers are about −0.8 and −1.5 eV at the PBE level, with an energy difference of 0.7 eV, reduced to *ca.* 0.4 eV upon inclusion of the D3(BJ) dispersion (see Table 2).

As can be seen in Table 2, the order of stabilities is inverse for the closed-shell Ag_2 case, as also found for the closed-shell Xe adatom (see ESI†). As discussed in previous work on noble gases on TiO_2[12,33,34,73] and Ag_2 on graphene,[68] the Ag_2–TiO_2 preferential adsorption is also significantly influenced by a subtle balance between short-range exchange–repulsion and long-range dispersion contributions: the exchange–repulsion is smaller on top of the Ti_{5f} site, allowing the Ag atoms to benefit from the attractive dispersion interaction with O_b atoms at both sides of the Ti_{5f} atom. The analysis of the projected density of states (PDOS) for the silver dimer (see Fig. 5) indicates that there is chemical mixing between Ag(4d) orbitals and O(2p) states of the support but no net charge-transfer. This finding is consistent with previous work on the Ag_4–TiO_2 (anatase) interaction.[69]

Obviously, the outer electrons of open-shell adsorbates are more prone to participate in chemical bonding with the support either by sharing or transferring them. Atomic charges were estimated with the Bader decomposition scheme.[74] The Bader charge on open-shell silver clusters was positive, having a value of about $+0.8|e|$, which is twice as large as found for the closed-shell Ag_2 cluster ($+0.4|e|$ only). The TiO_2 surface thus attracts more electronic charge from open-shell silver clusters.

In going from a single Ag adatom to Ag_3 and Ag_5 clusters, it can be observed that the well-depth values increase steeply (see Fig. 3 and Table 2), with the preferential adsorption along the row of O_b atoms being also very clear. From the PDOS of the supported open-shell species (see Fig. 5), the mixing between Ag(4d) and O(2p) orbitals (valence band) and between Ag(5s) and Ti(3d) orbitals (conduction band) can be observed, indicating the partial covalent nature of the adsorbate–surface interaction. However, the non-covalent vdW-type dispersion interaction is essential, contributing to the increase of the binding energy by 40–45% for Ag_3 and Ag_5 clusters.

As a second step, the geometries of supported Ag_3 and Ag_5 clusters were relaxed starting with those optimized for the free clusters with the PBE-D3(BJ) approach. As can can be seen in Fig. 4, both the (triangular) structure and the interaction energy (−2.5 eV) of the most stable Ag_3 isomer remain rather similar to those corresponding to the isolated cluster. Upon adsorption, the triangular Ag_3 structure becomes just a little bit tilted towards the Ti_{5f} site, signaling stability of the supported cluster. Also, the structure of the trapezoidal Ag_5 isomer is only slightly modified from that of the isolated cluster (see the middle panel of Fig. 4). The most pronounced change is in the stretching of the Ag–Ag bonds so that three Ag atoms now lie almost aligned with the O_b atoms along the surface normal direction. As found for the supported Ag_3 cluster, the diffusion of the Ag_5 cluster along the O_b row is rather constrained due to high energy barriers. For instance, when the cluster moves such that its center-of-mass lies in between two O_b atoms, the energy penalty is above 0.8 eV, indicating constrained diffusion and subsequent aggregation. Interestingly, we also found a more stable Ag_5 isomer (by *ca.* 1.3 eV) for which the planar trapezoid isomer transforms into a (slightly) pyramidal structure with four Ag atoms lying at the corners of a rectangle centered by one Ag atom atop a Ti_{5f} atom (see the right-hand panel of Fig. 4). Future work will consider the minimum-energy pathway from the trapezoidal to the pyramidal isomer.

3.3 Projected electronic density of states and absorption spectra

Using the cluster structures optimized at the PBE-D3(BJ) level, Fig. 5 shows the electronic density of states (EDOS) of the bare TiO_2(110) surface and the PDOS for the Ag_n/TiO_2(110) systems, as calculated with the hybrid HSE06 density functional, while the absorption spectra are presented in Fig. 6. As can be observed

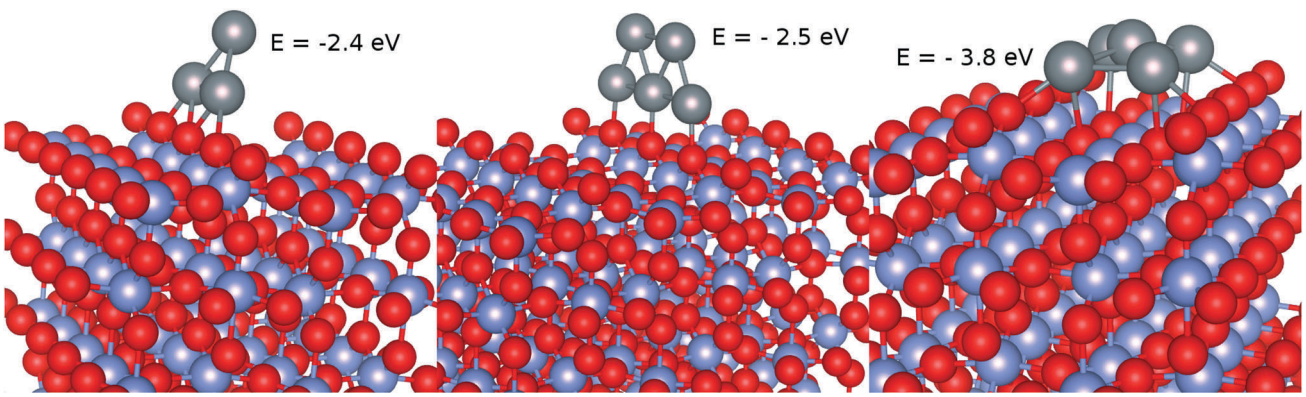

Fig. 4 Optimized geometries and binding energies of Ag_n clusters ($n \leq 5$) upon adsorption on the TiO_2(110) surface. Gray spheres represent silver atoms while red and blue spheres stand for oxygen and titanium atoms.

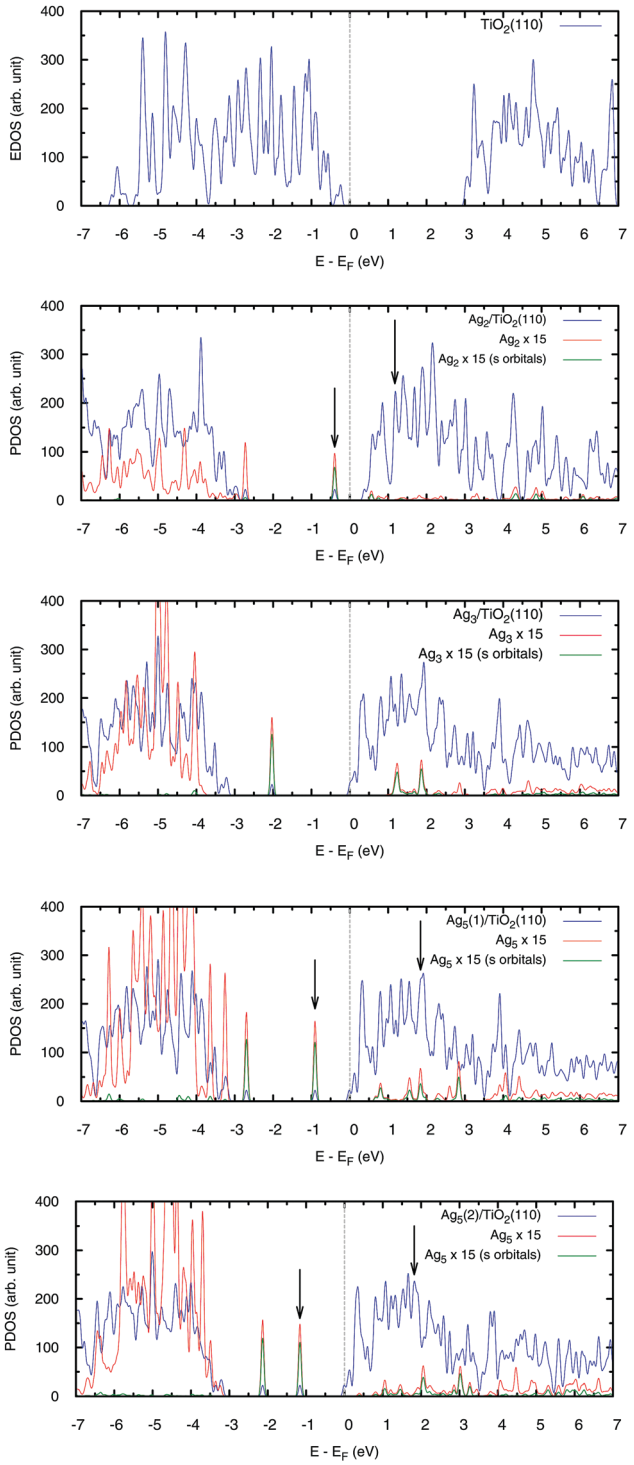

Fig. 5 EDOS of the TiO_2(110) surface and PDOS of the most stable Ag_n–TiO_2(110) systems obtained with the hybrid HSE06 functional, with Ag_5(1) and Ag_5(2) standing for the trapezoidal and pyramidal isomers (see Fig. 4). The zero of energy corresponds to the Fermi level, defined here as the highest occupied level. The arrows indicate the energies of the most responsible orbitals for the intense secondary peaks in the photo-absorption spectra (see Fig. 6).

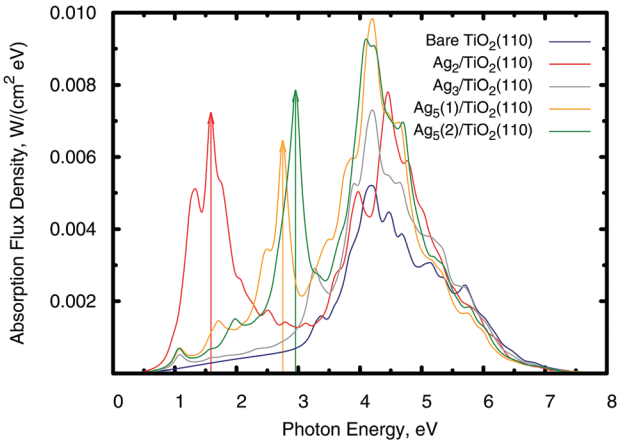

Fig. 6 Photo-absorption spectra of the TiO_2(110) surface, without adsorbates (shown in blue color) and with adsorbed Ag_n clusters. The most stable supported Ag_n clusters were considered, with Ag_5(1) and Ag_5(2) standing for the trapezoidal and pyramidal isomers (see Fig. 4). The arrows indicate the positions of the most intense secondary peaks across the near-infrared and visible regions of the solar spectrum.

in Fig. 5 (upper panel), our computational set-up provides an estimation of the band gap (3.3 eV) that agrees well with the experimental value (3.3 ± 0.5 eV from ref. 47). From Fig. 5, it can be seen that the supported Ag_n clusters add one or two sharp peaks in the band-gap region of TiO_2. These sharp peaks correspond to localized states in the Ag atomic clusters, as attested by the PDOS onto the Ag orbitals shown in Fig. 5. More specifically, these peaks arise from frontier orbitals mainly made of Ag(5s) orbitals but involving also hybridization with Ag(4p) orbitals. Notice also, that the Ag_n atomic clusters add intra-gap states closer to the bottom of the TiO_2 conduction band with increasing n. In fact, for n = 3 and 5, the conduction band begins to be populated giving an incipient metallic character to the system.

The intra-gap localized states have deep consequences for the light absorption behaviour. As shown in Fig. 6, the photo-absorption spectra develop broad absorption peaks in the visible (n = 5) and near-infrared (n = 2) spectra owing to photo-induced electronic transitions from the highest-energy localized orbitals to the conduction Ti(3d) states. The energy position of the frontier and the Ti(3d) orbitals involved in the transition with the largest oscillation strength are indicated by arrows in Fig. 5. In the case of the Ag_3 cluster, its only intra-gap state is far enough from the conduction band edge to contribute mainly to the absorption in the UV region. In this respect, notice also that the Ag_2 and Ag_5 clusters also enhance UV absorption in part owing to the contribution coming from the second lower energy intra-gap states present in these clusters. However, the observed enhancement of UV absorption comes not only because of the intra-gap peaks but also from the the energy band changes that the atomic clusters produce in the system.

The same electron transfer mechanisms found here for visible/near-infrared absorption have been proposed as being responsible for the photocatalytic hydrogen production enhancement observed after deposition of gold clusters onto TiO_2,[75] but instead of photo-transfer from localized orbitals of the adsorbate, the gold clusters are large enough to develop

their own conduction band as corroborated by the observation of a localized surface plasmon resonance band in the reflectivity. Notice also, that the localized nature of the Ag_n intra-gap states probably implies long lived hole excitations. Long lived photo-excitations are relevant to extract charge from photovoltaic devices. In this respect, the reduced density matrix treatment provides a pathway to calculate the hole lifetime, as previously shown for the Ag_3 cluster deposited on a Si(111) surface.[28] By the same token, the atomic clusters lack a properly developed populated conduction band so that they cannot sustain localized surface plasmons by themselves. However, since the Ag_n clusters give an incipient metal character to the system, probably already at room temperature, properly nanostructured Ag_n–TiO_2 may sustain localized surface plasmons, which have a well demonstrated beneficial effect in photovoltaic devices.[76]

Before concluding this section, we note that an interesting future direction of research would be to study the influence of the dispersion on single energy levels and the EDOS. For this purpose, it would be necessary to apply dispersion corrections depending on the electronic density such as the non-local vdW-DF[77] and vdW-DF2[78] approaches. Work along this line is currently in progress.

4 Conclusions

Motivated by the extraordinary properties of sub-nanometer silver clusters, we have presented a first-principles study of the stability and light absorption response of Ag_n clusters ($n \leq 5$) upon deposition on a TiO_2 surface. The vdW-corrected DFT-D3 scheme applied to analyze their stability has been first validated using a local version of the CCSD(T) method as well as the SAPT(DFT) approach, demonstrating excellent agreement (to within 10%). The DFT-D3 results show that the silver clusters are strongly bound to the support, with binding energies ranging from -0.9 eV for a single adatom to -3.8 eV for one Ag_5 isomer. The adsorbate–surface interaction is of polar-covalent nature, with the support attracting electronic charge from the cluster. The vdW dispersion also plays a crucial role, increasing very significantly the binding energies. The optimized structures of supported clusters differ slightly from those of their bare counterparts with the exception of one Ag_5 isomer. High energy penalties are found for the diffusion of the supported clusters so that high temperatures are predicted for their aggregation.

Using hybrid DFT calculations we have studied the influence of the Ag atomic clusters on the electronic density of states. One or two (depending on the number of Ag atoms) localized intra-gap states develop while at the same time the highest occupied level (at zero temperature) strongly shifts towards the system conduction band so that for $n = 3$ and 5 the initial conduction band state becomes populated.

Applying a scheme combining the hybrid DFT calculations with a reduced density matrix treatment, we have analyzed the light absorption response of the Ag_n–TiO_2 system. Besides increasing the intensity of the TiO_2 absorption spectra in the UV region, intense broad absorption peaks are also found in the infrared (the Ag_2–TiO_2 system) and the visible (the Ag_5–TiO_2 system) regions: an electron "jumps" from the Ag_n atomic cluster to the system conduction band leaving a hole in the cluster, when a photon is absorbed. The Ag_5-induced separation of photo-generated electrons and holes is expected to have a pronounced influence on the visible light photocatalytic activity of the modified TiO_2 material since hole–electron recombination is a key factor limiting the photocatalyst efficiency of unmodified TiO_2. Other surface locations for the atomic silver clusters are possible, with similar binding energies, and can be studied with the same methods. It is expected that the general features of light absorbance described here will remain the same for related structures. Also, as a "reporter" of the photocatalytic activity of the modified TiO_2 material, the photoreactivity of molecular oxygen adsorbed on the supported clusters will be addressed in future studies, following pioneering first-principles studies of O_2 photodesorption from bare TiO_2 surfaces,[79,80] including cluster-based embedding techniques.[81]

Conflicts of interest

There are no conflicts to declare.

Acknowledgements

This work has been partly supported by the Spanish Agencia Estatal de Investigación (AEI) and the Fondo Europeo de Desarrollo Regional (FEDER, UE) under Grant No. MAT2016-75354-P and COST Action CM1405 "Molecules in Motion" (MOLIM). The CESGA super-computer center (Spain) is acknowledged for having provided the computational resources used in this work. Work by D. A. M. has been partly supported by the National Science Foundation of the USA under grant. no. CHE-1445825 and by the HPC Computing Center of the University of Florida. MPdLC is greatly thankful to Arturo M. López-Quintela for very helpful suggestions and discussions.

References

1 Y. Piñeiro, D. Buceta, J. Rivas and A. M. López-Quintela, in *Metal Nanoparticles and Clusters*, ed. F. Deepak, Springer, 2018, pp. 1–30.
2 N. Vilar-Vidal, J. Rivas and M. A. López-Quintela, *ACS Catal.*, 2012, **2**, 1693–1697.
3 E. C. Tyo and S. Vajda, *Nat. Nanotechnol.*, 2015, **10**, 577–588.
4 P.-T. Chen, E. C. Tyo, M. Hayashi, M. J. Pellin, O. Safonova, M. Nachtegaal, J. A. van Bokhoven, S. Vajda and P. Zapol, *J. Phys. Chem. C*, 2017, **121**, 6614–6625.
5 N. Vilar-Vidal, J. R. Rey and M. A. López Quintela, *Small*, 2014, **10**, 3632–3636.
6 Y. A. Attia, D. Buceta, C. Blanco-Varela, M. B. Mohamed, G. Barone and M. A. López-Quintela, *J. Am. Chem. Soc.*, 2014, **136**, 1182–1185.

7 D. Buceta, N. Busto, G. Barone, J. M. Leal, F. Domínguez, L. J. Giovanetti, F. G. Requejo, B. García and M. A. López-Quintela, *Angew. Chem., Int. Ed.*, 2015, **54**, 7612–7616.
8 J. Neissa, C. Pérez-Arnaiz, V. Porto, N. Busto, E. Borrajo, J. M. Leal, M. A. López-Quintela, B. García and F. Domínguez, *Chem. Sci.*, 2015, **6**, 6717–6724.
9 S. Lee, C. Fan, T. Wu and S. L. Anderson, *J. Am. Chem. Soc.*, 2004, **126**, 5682–5683.
10 E. Loginov, L. F. Gómez and A. F. Vilesov, *J. Phys. Chem. A*, 2011, **115**, 7199–7204.
11 A. Volk, P. Thaler, M. Koch, E. Fisslthaler, W. Grogger and W. E. Ernst, *J. Chem. Phys.*, 2013, **138**, 214312.
12 M. P. de Lara-Castells, N. F. Aguirre, H. Stoll, A. O. Mitrushchenkov, D. Mateo and M. Pi, *J. Chem. Phys.*, 2015, **142**, 131101.
13 Q. Wu, C. J. Ridge, S. Zhao, D. Zakharov, J. Cen, X. Tong, E. Connors, D. Su, E. A. Stach, C. M. Lindsay and A. Orlov, *J. Phys. Chem. Lett.*, 2016, **7**, 2910–2914.
14 R. Fernández-Perea, Luis F. Gómez, C. Cabrillo, M. Pi, A. O. Mitrushchenkov, A. F. Vilesov and M. P. de Lara-Castells, *J. Phys. Chem. C*, 2017, **121**, 22248–22257.
15 Q. Guo, C. Zhou, Z. Ma, Z. Ren, H. Fan and X. Yang, *Chem. Soc. Rev.*, 2016, **45**, 3701–3730.
16 J. Schneider, M. Matsuoka, M. Takeuchi, J. Zhang, Y. Horiuchi, M. Anpo and D. W. Bahnemann, *Chem. Rev.*, 2014, **114**, 9919–9986.
17 Z. Zhang and J. T. Yates Jr., *Chem. Rev.*, 2012, **112**, 5520–5551.
18 M. A. Henderson, *Surf. Sci. Rep.*, 2011, **66**, 185–197.
19 P. Salvador and C. Gutierrez, *J. Phys. Chem.*, 1984, **88**, 3696–3698.
20 S. Grimme, J. Antony, S. Ehrlich and H. Krieg, *J. Chem. Phys.*, 2010, **132**, 154104.
21 S. Grimme, S. Ehrlich and L. Goerigk, *J. Comput. Chem.*, 2011, **32**, 1456–1465.
22 C. Riplinger and F. Neese, *J. Chem. Phys.*, 2013, **138**, 034106.
23 A. J. Misquitta, B. Jeziorski and K. Szalewicz, *Phys. Rev. Lett.*, 2003, **91**, 033201.
24 A. Heßelmann and G. Jansen, *Chem. Phys. Lett.*, 2003, **367**, 778–784.
25 J. Heyd, G. E. Scuseria and M. Ernzerhof, *J. Chem. Phys.*, 2003, **118**, 8207–8215.
26 A. V. Krukau, O. A. Vydrov, A. F. Izmaylov and G. E. Scuseria, *J. Chem. Phys.*, 2006, **125**, 224106.
27 V. May and O. Kühn, *Charge and Energy Transfer Dynamics in Molecular Systems*, Wiley-VCH, 2011.
28 D. S. Kilin and D. A. Micha, *J. Phys. Chem. Lett.*, 2010, **1**, 1073–1077.
29 T. Vazhappilly, D. S. Kilin and D. A. Micha, *J. Phys. Chem. C*, 2012, **116**, 25525–25536.
30 R. H. Hembree, T. Vazhappilly and D. A. Micha, *J. Chem. Phys.*, 2017, **147**, 224703.
31 N. F. Aguirre, D. Mateo, A. O. Mitrushchenkov, M. Pi and M. P. de Lara-Castells, *J. Chem. Phys.*, 2012, **136**, 124703.
32 W. Busayaporn, X. Torrelles, A. Wander, S. Tomić, A. Ernst, B. Montanari, N. M. Harrison, O. Bikondoa, I. Jourmard and J. Zegenhagen, *et al.*, *Phys. Rev. B: Condens. Matter Mater. Phys.*, 2010, **81**, 153404.
33 M. P. de Lara-Castells, H. Stoll and A. O. Mitrushchenkov, *J. Phys. Chem. A*, 2014, **118**, 6367–6384.
34 A. A. Tamijani, A. Salam and M. P. de Lara-Castells, *J. Phys. Chem. C*, 2016, **120**, 18126–18139.
35 N. G. Petrik and G. A. Kimmel, *Phys. Chem. Chem. Phys.*, 2014, **16**, 2338–2346.
36 B. Simard, P. A. Hackett, A. M. James and P. R. R. Langridge-Smith, *Chem. Phys. Lett.*, 1991, **186**, 415.
37 S. F. Boys and F. Bernardi, *Mol. Phys.*, 1970, **19**, 553–566.
38 J. P. Perdew, K. Burke and M. Ernzerhof, *Phys. Rev. Lett.*, 1996, **77**, 3865–3868.
39 A. Heßelmann, G. Jansen and M. Schütz, *J. Chem. Phys.*, 2005, **122**, 014103.
40 A. J. Misquitta, R. Podeszwa, B. Jeziorski and K. Szalewicz, *J. Chem. Phys.*, 2005, **123**, 214103.
41 K. Patkowski, K. Szalewicz and B. Jeziorski, *J. Chem. Phys.*, 2006, **125**, 154107.
42 B. Jeziorski, R. Moszynski, A. Ratkiewicz, S. Rybak, K. Szalewicz and H. L. Williams, in *Mehods and Techniques in Computational Chemistry; METECC94*, ed. E. Clementi and D. Reidel, Publishing Company, STEF, Cagliari, 1993, vol. B, p. 79.
43 P. Deák, B. Aradi and T. Frauenheim, *Phys. Rev. B: Condens. Matter Mater. Phys.*, 2011, **83**, 155207.
44 J. Anderson, V. de Walle and G. Chris, *Phys. Status Solidi B*, 2010, **248**, 799–804.
45 A. Janotti, J. B. Varley, P. Rinke, N. Umezawa, G. Kresse and C. G. Van de Walle, *Phys. Rev. B: Condens. Matter Mater. Phys.*, 2010, **81**, 085212.
46 V. Francesc, L. Oriol, C. K. Kyoung, Y. L. Jin and I. Francesc, *J. Comput. Chem.*, 2017, **38**, 781–789.
47 Y. Tezuka, S. Shin, T. Ishii, T. Ejima, S. Suzuki and S. Sato, *J. Phys. Soc. Jpn.*, 1994, **63**, 347–357.
48 D. S. Kilin and D. A. Micha, *J. Phys. Chem. C*, 2009, **113**, 3530–3542.
49 D. A. Micha, *Adv. Quantum Chem.*, 2015, **71**, 195–220.
50 D. A. Micha, *Adv. Quantum Chem.*, 2017, **14**, 107–127.
51 K. Ozawa, S. Yamamoto, R. Yukawa, R.-Y. Liu, N. Terashima, Y. Natsui, H. Kato, K. Mase and I. Matsuda, *J. Phys. Chem. C*, 2018, **122**, 9562–9569.
52 T. Vazhappilly and D. A. Micha, *J. Phys. Chem. C*, 2014, **118**, 4429–4436.
53 D. E. Woon and T. H. Dunning, Jr., *J. Chem. Phys.*, 1994, **100**, 2975–2988.
54 K. A. Peterson and C. Puzzarini, *Theor. Chem. Acc.*, 2005, **114**, 283.
55 K. A. Peterson, D. Figgen, E. Goll, H. Stoll and M. Dolg, *J. Chem. Phys.*, 2003, **119**, 11113.
56 D. Figgen, G. Rauhut, M. Dolg and H. Stoll, *Chem. Phys.*, 2005, **311**, 227.
57 F. Neese, *Wiley Interdiscip. Rev.: Comput. Mol. Sci.*, 2018, **8**, e1327.
58 H. J. Werner, P. J. Knowles, G. Knizia, F. R. Manby, M. Schütz, P. Celani, T. Korona, R. Lindh, A. O. Mitrushchenkov, G. Rauhut, *et al.*, *MOLPRO, version2012.1, a package of ab initio programs*, see http://www.molpro.net.

59 M. Grüning, O. V. Gritsenko, S. V. A. van Gisbergen and E. J. Baerends, *J. Chem. Phys.*, 2001, **114**, 652–660.
60 S. Lias, in *NIST Chemistry WebBook, NIST Standard Reference Database Number 69*, ed. P. Linstrom and W. Mallard, National Institute of Standards and Technology, Gaithersburg, 2005, ch. Ionization Energy Evaluation.
61 A. Borodin and M. Reichling, *Phys. Chem. Chem. Phys.*, 2011, **13**, 15442–15447.
62 G. Kresse and J. Furthmüller, *Phys. Rev. B: Condens. Matter Mater. Phys.*, 1996, **54**, 11169.
63 G. Kresse and D. Joubert, *Phys. Rev. B: Condens. Matter Mater. Phys.*, 1999, **59**, 1758.
64 P. E. Blöch, *Phys. Rev. B: Condens. Matter Mater. Phys.*, 1994, **50**, 17953.
65 H. J. Monkhorst and J. D. Pack, *Phys. Rev. B: Solid State*, 1976, **13**, 5188–5192.
66 H. Stoll, *J. Chem. Phys.*, 1992, **97**, 8449–8454.
67 A. Kubas, D. Berger, H. Oberhofer, D. Maganas, K. Reuter and F. Neese, *J. Phys. Chem. Lett.*, 2016, **7**, 4207–4212.
68 M. P. de Lara-Castells, A. O. Mitrushchenkov and H. Stoll, *J. Chem. Phys.*, 2015, **143**, 102804.
69 A. R. Puigdollers, P. Schlexer and G. Pacchioni, *J. Phys. Chem. C*, 2015, **119**, 15381–15389.
70 M. Chen, J. E. Dyer, K. Li and D. A. Dixon, *J. Phys. Chem. A*, 2013, **117**, 8298–8313.
71 V. Bonacicić-Koutecky, V. Veyret and R. Mitrić, *J. Chem. Phys.*, 2001, **115**, 10450–10460.
72 T. L. Haslett, K. A. Bosnick and M. Moskovits, *J. Chem. Phys.*, 1998, **108**, 3453–3457.
73 M. P. de Lara-Castells, N. F. Aguirre and A. O. Mitrushchenkov, *Chem. Phys.*, 2012, **399**, 272–280.
74 R. F. W. Bader, *Chem. Rev.*, 1991, **91**, 893–928.
75 C. Gomes Silva, R. Juárez, T. Marino, R. Molinari and H. García, *J. Am. Chem. Soc.*, 2011, **133**, 595–602.
76 K. Ueno, T. Oshikiri, Q. Sun, X. Shi and H. Misawa, *Chem. Rev.*, 2018, **118**, 2955–2993.
77 M. Dion, H. Rydberg, E. Schröder, D. C. Langreth and B. I. Lundqvist, *Phys. Rev. Lett.*, 2004, **92**, 246401.
78 K. Lee, E. Eamonn, L. Kong, B. I. Lundqvist and D. C. Langreth, *Phys. Rev. B: Condens. Matter Mater. Phys.*, 2010, **82**, 081101(R).
79 M. P. de Lara-Castells and J. L. Krause, *J. Chem. Phys.*, 2003, **118**, 5098–5105.
80 M. P. de Lara-Castells, A. O. Mitrushchenkov, O. Roncero and J. L. Krause, *Isr. J. Chem.*, 2005, **45**, 59–76.
81 M. P. de Lara-Castells and A. O. Mitrushchenkov, *J. Phys. Chem. C*, 2011, **115**, 17540–17557.